

Multiple limit cycles in laser interference transduced resonators

David Blocher*, Richard H. Rand, Alan T. Zehnder

Field of Theoretical and Applied Mechanics, Cornell University, Ithaca, NY 14853, USA

ARTICLE INFO

Article history:

Received 23 September 2011

Received in revised form

18 February 2013

Accepted 19 February 2013

Available online 27 February 2013

Keywords:

MEMS

Limit cycle

Hopf bifurcation

Numerical continuation

Resonator

ABSTRACT

Nanoscale resonators whose motion is measured through laser interferometry are known to exhibit stable limit cycle motion. Motion of the resonator through the interference field modulates the amount of light absorbed by the resonator and hence the temperature field within it. The resulting coupling of motion and thermal stresses can lead to self-oscillation, i.e. a limit cycle. In this work the coexistence of multiple stable limit cycles is demonstrated in an analytic model. Numerical continuation and direct numerical integration are used to study the structure of the solutions to the model. The effect of damping is discussed as well as the properties that would be necessary for physical devices to exhibit this behavior.

© 2013 Elsevier Ltd. All rights reserved.

1. Introduction

Due to their high frequencies, ease of integration with traditional electronics and potential for low cost batch fabrication, MEMS resonators have found a variety of uses in the past decade from electrical filters [1] to mass detection sensors [2], gyroscopes [3,4] and reference oscillators [5]. In such applications, the frequency or phase of oscillation of the MEMS device carries information about the quantity of interest. To obtain periodic motion, devices are often driven using an externally modulated drive. Such designs require an external highly stable frequency source, which increases sensor cost. Active feedback electronics may also be used to create sustained oscillations [6] though will become increasingly challenging as device frequencies continue to increase. Self-resonant systems, or limit cycle oscillators, offer a promising alternative for achieving periodic motion and have been demonstrated in MEMS opto-mechanical systems.

Langdon and Dowe [7] first demonstrated optically driven self-oscillation in a MEMS device. They showed that an optically thin MEMS device suspended over a reflective substrate sets up a Fabry–Pérot interferometer which couples absorption of light to displacement of the device. Thus, illuminating MEMS beams with a continuous wave (CW) unmodulated laser causes optical–thermal–mechanical feedback.¹ The sign of the feedback gain is determined by the length of the interference cavity, or wavelength of the light used for illumination. For negative feedback

gain, feedback increases damping and is termed cavity- or self-cooling [8,9]. For positive feedback, back-action reduces damping. In this case, when the laser intensity is low, the beam bends statically, but for laser powers above a threshold power, P_{Hopf} , the beam exhibits a large amplitude self-oscillation. Later work examined the necessary conditions for self-oscillation [14–16]. See [17] for an overview of limit cycles in thermo-optically driven MEMS, as well as [18–23] for other works in the area.

A typical experimental setup is shown schematically in Fig. 1. Devices are fabricated from a thin film stack to create an optically thin resonator suspended over a thick substrate. A CW laser is focused on the resonator,² mounted in vacuum to reduce damping. The resonator-gap-substrate system sets up a Fabry–Pérot interferometer whose absorbed signal depends on the device gap. As the resonator moves through the interference field, it modulates the reflected signal which is measured in an AC-coupled photodiode. This general setup has been used to excite and study oscillations in cantilevers, clamped–clamped beams, disks and domes [24,17,25].

Previous work [17,26] on modeling the dynamics of limit cycle oscillations in optically driven MEMS resonators has assumed small displacement and expanded the function describing the interference field in a power series, losing the periodicity in the process. In this work, we treat the case where displacement is not small and show that a periodic interference field suggests the coexistence of multiple stable limit cycles. To our knowledge, the

* Corresponding author. Tel.: +1 607 255 0824; fax: +1 607 255 2011.

E-mail address: dbb74@cornell.edu (D. Blocher).

¹ For beams with low absorption, light pressure dominates photo-thermal stress [8–13] leading to direct optical-mechanical feedback.

² Though past work has used external HeNe lasers and photodiodes, co-integration with wafer level vertical cavity surface emitting lasers (VCSELs) and photodiodes would enable truly stand-alone sensors, and eliminate the need for alignment or collimating optics.

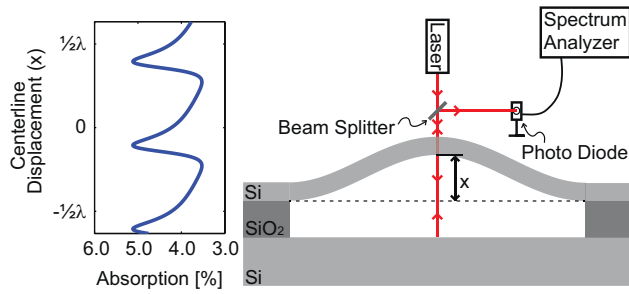


Fig. 1. Cross-sectional view of an interferometrically transduced clamped-clamped MEMS beam. Inset is a plot of the laser energy absorbed as a function of the centerline displacement (x) measured with respect to the undeflected configuration. As the beam deflects, it changes the gap to substrate and modulates the absorption. Thus the interferometer couples heating to displacement. The absorption is periodic in $\lambda/2$.

coexistence of multiple *stable* limit cycles have not been predicted or seen experimentally in the previous work on MEMS.³ Devices exhibiting multiple stable limit cycles would allow for tuning between distinct frequency bands. For example, in applications such as GPS receivers narrow tuning within a band would be required to overcome drift or process variation, and tuning between bands would allow a single device to cover both L1 and L2 broadcast frequencies. On the other hand, extraneous stable motions could be problematic if a device designed to operate in one limit cycle was found to operate in a different limit cycle with a different frequency and amplitude.

In the following sections, the resonators are described, the equations of motion used to model them are derived and model parameters are identified. Then continuation and direct integration results are presented and discussed. Since small displacement is not assumed, approximate analytic methods (Lindstedt's method, harmonic balance) give poor predictions, thus no analytic results are presented. Lastly, conclusions are drawn about the properties of corresponding physical devices in which multiple stable limit cycles would be possible.

2. Theoretical model

The equations that follow are applicable to any interferometrically driven MEMS device with a temperature dependent stiffness and direct thermal-mechanical coupling, but here a clamped-clamped beam is modeled to illustrate the phenomenon. A similar model has been used to describe the motion of optically excited disks, dome oscillators and beams [24,17,27,28]. See [24,29] for a more detailed discussion. Although the devices have spatially varying fields, first-mode vibration is assumed, and the centerline displacement (x) as depicted in Fig. 1 is modeled as a one degree-of-freedom oscillator. A quasi-static temperature field is assumed, and the average temperature in the device (T) is modeled using a lumped thermal model. No external forcing is applied to the system. To begin with, we describe the mechanical model (1).

Though membrane stress is neglected in linear beam theory, it is an important non-linearity for high curvature deformations in structures. For pre-buckled beams subject to out of plane loads, the slope of a force vs. displacement curve increases with displacement due to membrane stresses, a phenomenon called "hardening." Membrane stress has been shown to come into an

oscillator model of first mode vibration as a cubic stiffness ($\tilde{\beta}x^3$) which is hardening ($\tilde{\beta} > 0$) for pre-buckled beams [30] and softening ($\tilde{\beta} < 0$) for post-buckled beams [31]. As a result, a cubic stiffness term is included to incorporate the effect of membrane stiffness.

The temperature above ambient in the beam (T) leads to an increase in compressive stress at the support needed to counteract thermal strain. It is known that the first mode frequency of a clamped-clamped beam decreases monotonically as the compression is increased until it reaches zero frequency at the buckling load [32]. Thus the stiffness of the beam to out of plane displacements is a decreasing function of temperature. In order to account for the dependence of frequency on temperature the linear spring stiffness is modeled as a decreasing function of temperature: $k = k_0(1 - \tilde{c}_1 T)$, where the spring stiffness temperature coefficient (\tilde{c}_1) determines how strongly the frequency depends on temperature. This recovers the theoretical resonant frequency exactly for pre-buckled beams [32] and approximately for post-buckled beams [33].

Finally, it has been observed that heating of cantilever beams causes static deflection due to stress gradients at the anchor points [34]. FEM modeling indicates that the same is true for clamped-clamped beams [35]. To incorporate this direct change in displacement due to temperature a term proportional to the temperature ($\tilde{c}_2 T$) is included in the mechanical model which shifts the equilibrium solution as the temperature increases. The thermo-mechanical coupling coefficient (\tilde{c}_2) is the deflection for a unit temperature change. Including a damping term, along with the terms previously described and non-dimensionalizing, gives the following mechanical model:

$$\ddot{z} + \frac{\dot{z}}{Q} + (1 - c_1 T)z + \beta z^3 = c_2 T, \quad (1)$$

where z is the centerline displacement scaled by the laser wavelength ($z = x/\lambda$), time is rescaled by the linear resonant frequency ($\tau = t\omega_0$), overdots denote derivatives with respect to non-dimensional time τ , and the parameters $\tilde{\beta}$, \tilde{c}_1 , \tilde{c}_2 have been transformed to the dimensionally appropriate β , c_1 , c_2 .

The resonator is assumed to heat up due to laser absorption and cool down due to Newton's law of cooling, giving the following equation governing the average temperature in the beam (T):

$$\dot{T} = -BT + HP_{absorbed}(z), \quad (2)$$

where B is the cooling rate due to conduction, H is the inverse of the lumped thermal mass and $P_{absorbed}(z)$ is the energy absorbed due to interferometric heating. Once again, overdots represent derivatives with respect to non-dimensional time τ . Note that the absorption function $P_{absorbed}(z)$ depends on the properties of the interferometer for a given deflection (z) and is proportional to the applied laser power. $P_{absorbed}(z)$ can be described numerically using an optical model presented in [36]. The resulting function is periodic with period $\lambda/2$ in x (or $1/2$ in z) and is approximated by

$$P_{absorbed}(z) = P[\alpha + \gamma \sin^2(2\pi(z - z_o))] \quad (3)$$

with fitting parameters α , γ and z_o . Eqs. (1)–(3) form a system of two coupled ordinary differential equations and one algebraic equation to model the first mode of vibration of a MEMS resonator.

In [17,26], Eq. (3) was approximated by replacing the sine function by the first two terms of its Taylor series. This permitted an approximate analytic treatment using perturbations, but limited the applicability of the results to small amplitudes of vibration. In the present work this limitation is removed, and the analytic treatment of [17,26] is replaced by numerical treatment using the continuation (bifurcation) software AUTO [37,38]. The

³ It has been shown that first or second mode vibrations could be excited into self-oscillation by varying the cavity length [16].

result is a dynamical system which is richer in dynamical phenomena (multiple limit cycles and associated bifurcations). From a physical point of view, the reason for the increase in complexity lies in the fact that as z increases, the absorption of light energy varies periodically (i.e. sinusoidally) with z due to interference. By replacing the sine function in Eq. (3) by a cubic approximation, the analysis in [17,26] eliminated this aspect of the physics, and with it much of the dynamical behavior.

In the next section, the parameter estimation process is described and parameters are established for a 201 nm thick, 10 μm long clamped–clamped silicon beam with 400 nm gap to substrate, subjected to 50 MPa of pre-compression.

3. Parameter estimation

Estimation of the physical, thermal and optical parameters is done using a number of different analyses. The optical parameters α , γ and z_0 are least squares fit to the numerical results from the model presented in [36]. Given the complex index of refraction of the materials as well as the resonator thickness and gap to substrate, the algorithm given in [36] solves Maxwell’s equations to determine the percentage of laser energy absorbed in and reflected from the resonator. The gap to substrate is varied to account for deflection of the device, giving a result seen in Fig. 1. For the 201 nm thick silicon device with 400 nm un-deflected gap to substrate, we estimate $\alpha \approx 0.035$, $\gamma \approx 0.011$ and $z_0 \approx 0.18$.

The mechanical parameters are fit as follows: first the devices under test are driven at low amplitude in vacuum and their resonance curve is measured. The quality factor (Q) is determined by fitting the resonance curve to a Lorentzian and is estimated to be $Q=13,800$. Given the low damping, the natural frequency (ω_0) is taken to be equal to the resonant frequency ($\omega_r=9.96$ MHz) which is used to non-dimensionalize the equations. The spring stiffness temperature coefficient ($c_1=0.00475$ K^{-1}) is determined by taking a Taylor series expansion of the frequency–compression relation given in [32], using linear thermoelasticity to convert between temperature above the ambient and compression. The cubic stiffness ($\beta=4.65$) is estimated using an FEM analysis in which a normal load of 0–10 μN is applied at the center of a clamped–clamped beam. The load–displacement curve is least squares fit to $F=kz+\beta z^3$ using the appropriate non-dimensionalization.

The thermal parameters are also fit using an FEM analysis. The beam and a large volume of the surrounding substrate are modeled in 3D. The temperature is assumed to be zero at the outer boundary and a Heaviside unit flux is applied at the center of the beam. The inverse lumped thermal mass (H) is related to the slope of the temperature at time $t=0$ ($\dot{T}|_{t=0}=H$) and the cooling rate due to conduction (B) is related to the steady state average temperature ($\lim_{t \rightarrow \infty} T(t)=H/B$).

To determine c_2 , equivalent thermal stresses are calculated from the steady state temperature field and applied to the mechanical model. The normalized centerline deflection for unit temperature rise is the thermal coupling coefficient (c_2). See Table 1 for a full list of material properties used for parameter estimation and Table 2 for estimated model parameters.

4. Continuation results

The continuation tool AUTO 2000 [37,38] is used to examine the structure of solutions to Eqs. (1)–(3). This software package is commonly used in the bifurcation analysis of differential equations and algebraic systems. Using AUTO 2000 we track the

Table 1
Material properties used in parameter estimation.

Material properties	Si	SiO ₂
Density (kg/m ³)	2420	2200
Poisson ratio	0.279	0.17
Young’s modulus [GPa]	130	70
CTE (ppm/K)	2.5	0.5
Thermal conductivity (W/m*K)	170	1.38
Specific heat capacity (J/kg*K)	712	1120
Index of refraction	3.882–0.019i	N/A

Table 2
Estimated parameters used in continuation and integration of model equations, for 201 nm thick, 10 μm long beams, subject to 50 MPa of pre-compression.

Model parameters	
Q	13,800
c_1	4.75×10^{-3} (K^{-1})
c_2	1.37×10^{-5} (K^{-1})
β	4.65
H	4410 (K/W)
B	0.152
γ	0.011
α	0.035
z_0	0.18

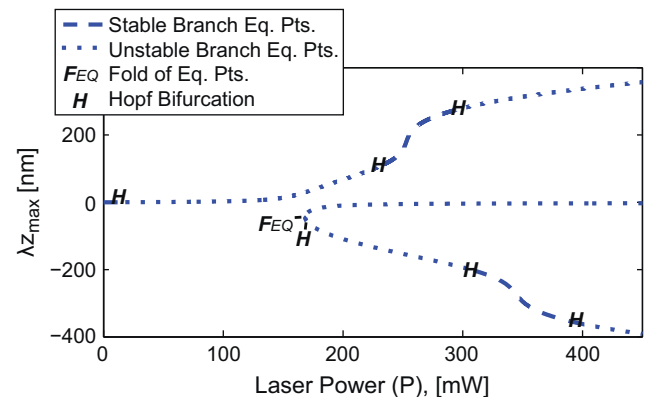


Fig. 2. AUTO generated bifurcation diagram of the system showing location and stability of equilibrium solutions as a function of laser power (P). Limit cycle branches emerging from Hopf bifurcations (H) are shown in Fig. 9.

change in the equilibrium and periodic solutions as the laser power is varied.

We begin with $P=0$ which has known equilibrium solution ($z=0, \dot{z}=0, T=0$). This equilibrium solution is continued in P , monitoring the eigenvalues of the Jacobian of the linearized system for Hopf-bifurcations. For low laser power, there is a unique stable equilibrium solution with small centerline displacement. As the laser power is increased to $P \approx 18$ mW, this equilibrium solution loses stability in a Hopf bifurcation leading to self-oscillation. As the power is increased further, the equilibrium solution branch begins to lift up from $z_{eq}=0$ and a second branch of equilibrium solutions is born at $P \approx 168$ mW in a fold of equilibrium points. An equilibrium point along this branch is computed numerically using a root finding method and then is used as a starting point for continuation of the branch. See Fig. 2 for a plot of the equilibrium branches along with Hopf-bifurcation points at which limit cycles are born. This behavior in the position and number of equilibria is caused by asymmetric buckling in the

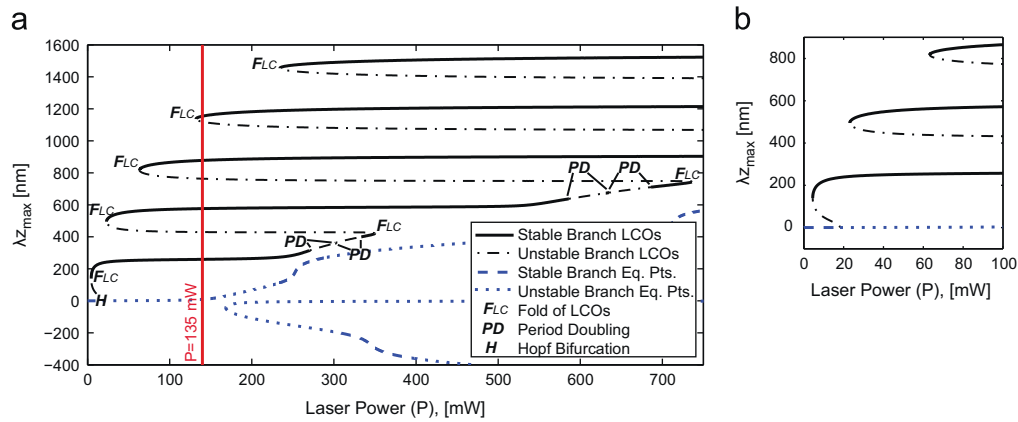


Fig. 3. AUTO generated bifurcation diagram (a) showing the two branches of equilibrium solutions as well as the branch of limit cycles born in the first Hopf bifurcation. Included is a zoom view (b) of the bifurcation diagram for low laser power. The intersection of a vertical line with the equilibrium or limit cycle branches indicates the solutions possible at a given laser power. See Fig. 4 for a phase portrait of the limit cycles and equilibrium solutions for $P=135$ mW.

model. Hopf bifurcations along the branches of equilibria alter the usual buckling stability result – that the unbuckled state is unstable and the buckled states are stable.

Next, we turn our attention to the limit cycle oscillations born in Hopf bifurcations. The continuation is restarted at each Hopf bifurcation and the emerging limit cycle is followed, allowing the power P and frequency of oscillation ω to vary. Following the limit cycle branch born in the first Hopf bifurcation, we see a series of folds of limit cycles in which stable and unstable limit cycles coalesce or divide (see Fig. 3), in addition to regions of period doubling which are discussed later. To display equilibrium points and limit cycles on the same bifurcation diagram, the maximum displacement attained during one cycle (z_{max}) is used as the dependent variable for limit cycles. This measure includes the amplitude plus a small mean value roughly equal to the displacement of the equilibrium solution from which the motion was born. Note that for a given laser power, the amplitudes of stable limit cycles differ by roughly the period of the interferometer, $\lambda/2 \sim 316$ nm. Thus the multiplicity of stable limit cycles is due to periodicity in the interference field, and each higher amplitude stable limit cycle shows motion between similar points in the phase of the interference field, but includes more or less periods. For example, if the lowest amplitude limit cycle shows motion between one peak of absorption in the interference field and the first subsequent peak in the interference field, then the second lowest amplitude limit cycle shows motion between one peak of the absorption in the interference field and the second subsequent peak (see Fig. 1). See Fig. 4 for a phase portrait of the equilibrium solution and limit cycles for $P=135$ mW when a stable and unstable limit cycle have just been born in a fold of limit cycles.

The period of oscillation along the first Hopf branch is depicted in Fig. 5. Note that the limit cycle initially has non-dimensional period of $\sim 2\pi$. As the laser power is increased two competing factors influence the period of oscillation. The temperature dependence of the linear stiffness causes the period to increase with temperature and so the period increases with laser power for a given stable limit cycle. At the same time, the cubic stiffness due to membrane stresses causes the period to decrease with increasing amplitude of oscillation. Thus at a fixed laser power, high amplitude limit cycles have lower periods. Competition between different frequency tuning mechanisms has been noted elsewhere [24].

It is numerically observed that as damping is increased, high amplitude limit cycles become unattainable at low laser power. Increased damping flattens out these curves in the first Hopf branch, reducing the number of stable limit cycles accessible at a given laser power (see Fig. 6). For sufficiently high damping, the

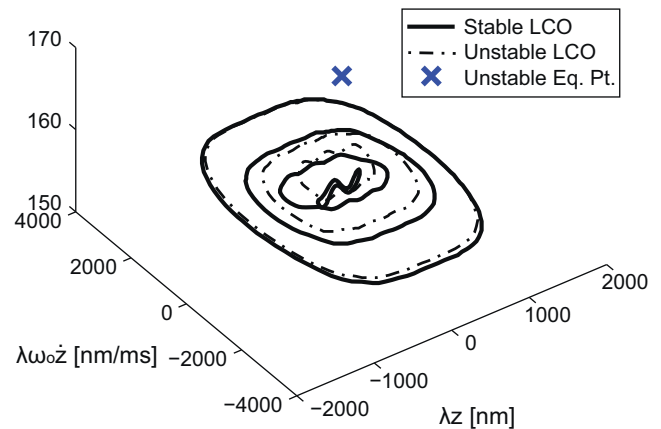


Fig. 4. Plot of the equilibrium and periodic solutions for $P=135$ mW. Note that large amplitude stable and unstable motions have just been born in a fold of limit cycles. See Fig. 3 for the accompanying bifurcation diagram.

Hopf bifurcation becomes supercritical and a unique stable limit cycle exists in this branch for $P > P_{Hopf}$.

Although the results presented here are for $10 \mu\text{m}$ beams subject to 50 MPa of pre-compression, we have estimated parameters for beams of length 7, 10, 15 and $20 \mu\text{m}$ with varying amounts of pre-compression. Continuation of the model equations using these parameters shows that multiplicity of stable limit cycles in the first Hopf branch is a *robust feature of the model* for lightly damped pre-buckled beams and occurs at laser powers which are realizable in experimental setups. In the following section, we describe the rest of the bifurcation structure for $10 \mu\text{m}$ beams, including bifurcations occurring at laser powers above the thermal buckling power. We also describe the jump phenomenon associated with the destruction of stable limit cycles.

5. Complete bifurcation diagram

In this section we build up the complete picture of the bifurcation structure, by describing each additional bifurcation separately. To begin with, we return to the regions of period doubling along the first Hopf branch (see Fig. 3). Here we see that as we increase the laser power, our original limit cycle goes unstable and a new stable limit cycle is born with twice the period of the original. Continuing this new limit cycle, there is a cascade of period doubling where this process continues with

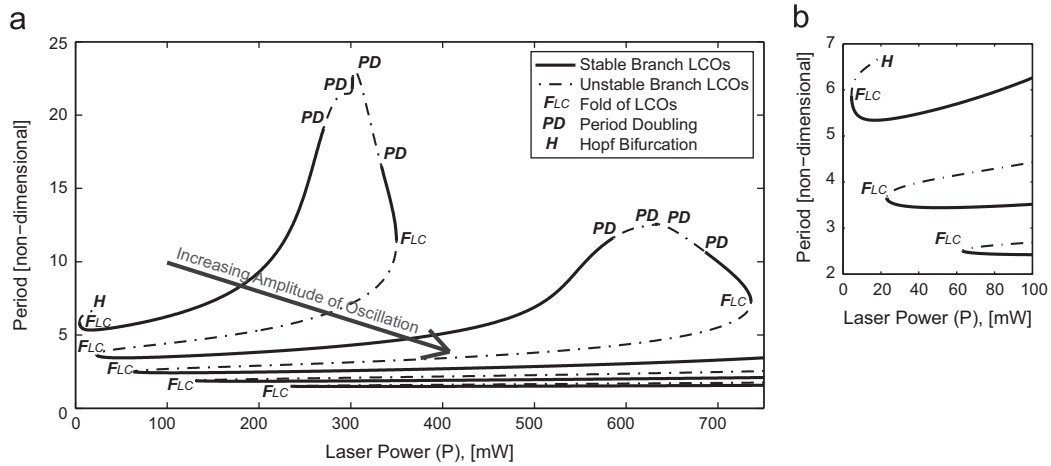


Fig. 5. The period of oscillation (a) along the branch of limit cycles born in the first Hopf. Included is a zoom view (b) of the period for low laser power. Note that the limit cycle is born with non-dimensional period $\sim 2\pi$ at the point marked H.

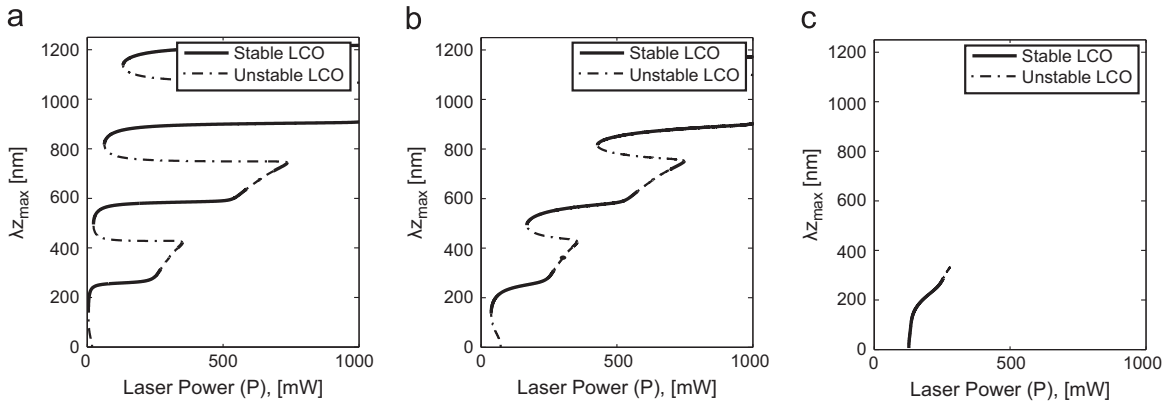


Fig. 6. Effect of damping: AUTO generated bifurcation diagram showing the branch of limit cycles born in the first Hopf bifurcation. The same model parameters are used as before, except the quality factor (Q) is reduced by a factor of 10 between each subplot. Note that the increased damping increases the laser power at which self-oscillation becomes possible and also flattens out the curves in the first Hopf branch. For $Q=140$, the Hopf bifurcation has become supercritical and there is a unique stable limit cycle, which quickly leads to period doubling and dies in a homoclinic bifurcation (not shown).

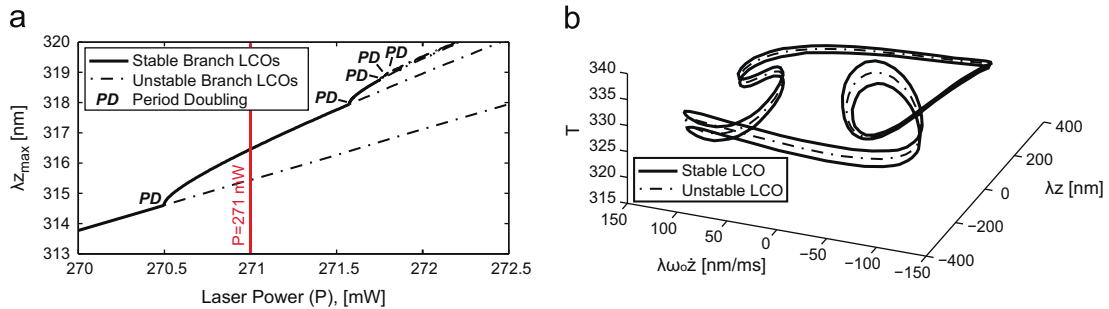


Fig. 7. Bifurcation diagram (a) of a cascade of period doubling for high laser power. Only the first five period doubling bifurcations are tracked numerically, though more are believed to exist. A phase portrait (b) just after the first period doubling bifurcation shows that the original limit cycle (one-loop) has gone unstable and a new stable cycle is born which traverses two loops before closing.

increasing frequency as we increase the laser power (see Fig. 7). Direct numerical integration is used to verify the existence of these special solutions. Period doubling is a well-known route to chaos, and chaos has been experimentally observed in the forced vibration of buckled beams [40], thus it is likely that chaos exists in the model in this range of laser powers.

For all the parameter sets studied, there were additional Hopf bifurcations from the equilibrium branches for laser powers above the buckling power. Following the limit cycle emerging from the second Hopf bifurcation, we see a fold of limit cycles and then the cycle coalesces with an unstable equilibrium point in a

homoclinic bifurcation. See Fig. 8 for a bifurcation diagram of this region and a phase portrait just before the homoclinic bifurcation. Accounting for the limit cycles born in the other Hopf bifurcations gives a complete bifurcation diagram shown in Fig. 9.

6. Jump phenomenon

Finally direct integration is used to illustrate the hysteresis possible in the system. Although the bifurcation structure illustrates the types of stable and unstable behaviors possible in the model, it

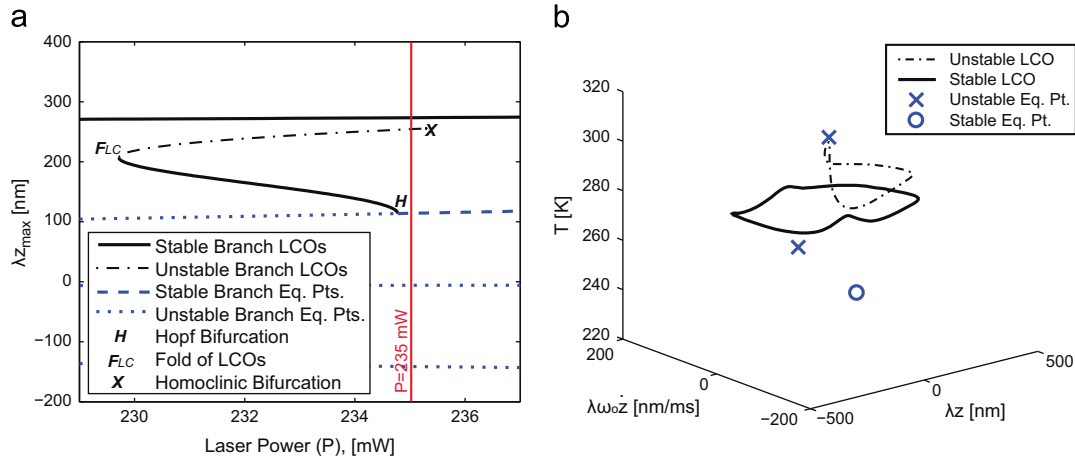


Fig. 8. Portion of the bifurcation diagram (a) in the region of the second Hopf point (after the thermal buckling point as seen in Fig. 9) and phase portrait (b) of the system just before the homoclinic bifurcation. The unstable limit cycle has developed a kink as it approaches the stable and unstable manifold of an equilibrium point. Included is the neighboring limit cycle from the first Hopf branch, though higher amplitude limit cycles are omitted.

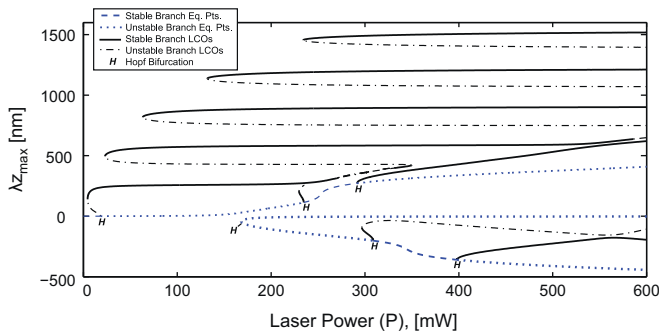


Fig. 9. Complete bifurcation diagram of the system. Note that the limit cycle oscillation born in a Hopf bifurcation in the elbow of the fold of equilibria dies so quickly in a homoclinic bifurcation that is not visible on the bifurcation diagram at this scale.

does not tell us which behaviors would be seen experimentally as we change the laser power – a question dealing with the basins of attraction for different stable behaviors. We explore these basins using direct integration. For each Hopf bifurcation or fold of limit cycles where an equilibrium solution loses stability or stable motion disappears, respectively, we use a point along that motion as an initial condition, increase or decrease the laser power slightly beyond the bifurcation and integrate until the trajectory settles onto a new steady behavior. See Fig. 10 for a plot of the jump phenomenon. As we quasi-statically increase the laser power from zero beyond the first Hopf bifurcation at $P \sim 18$ mW, the beam begins to oscillate in the lowest amplitude limit cycle. Once oscillating, we have to decrease the power below the lowest fold of limit cycles at $P \sim 4.5$ mW in order to jump back onto the stable equilibrium solution. At each fold of limit cycles along the first Hopf branch, jumps occur up to the next highest amplitude stable limit cycle when increasing the laser power, or down to the next lowest amplitude stable limit cycle when decreasing the laser power. Entering the region of period doubling, stable n -cycles give rise to stable $2n$ -cycles and so there are no jumps. However, it is unclear if stable periodic motions exist over the entire interval or if there are regions of chaos.

7. Comparison with previous work

Previous work [17,26] on modeling limit cycle oscillations in optically driven MEMS resonators has assumed small displacement,

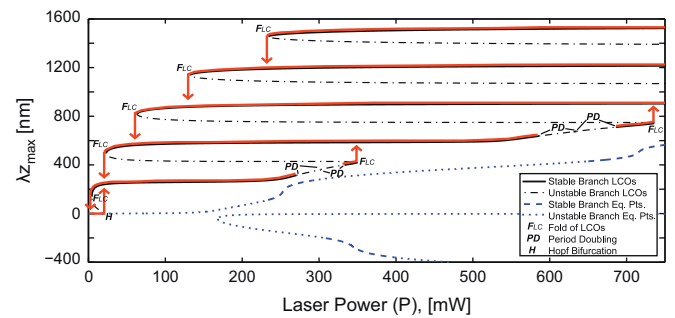


Fig. 10. Jump phenomenon in the first Hopf branch.

and expanded the optical Eq. (3) in a power series losing the periodicity in the process, but making the equations amenable to approximate analytic methods. This small displacement approximation predicts a single Hopf bifurcation, either subcritical or supercritical, leading to a stable/unstable pair or single stable limit cycle, respectively. Thus series expanding the optical equation suppresses secondary Hopf bifurcations and folds of limit cycles. For comparison, a bifurcation diagram for Eqs. (1) and (2) is given in Fig. 11, where the parameters from Table 2 are used but Eq. (3) has been Taylor expanded in z , keeping the first two terms.

8. Conclusion

A MEMS device illuminated within an interference field will self-oscillate due to feedback between absorption and displacement. Models in the form of coupled differential equations have been used to describe the dynamics of such vibrations [17,20,41,24,26–28,15], and analyzed under the assumption of small displacement. In this work, we show that if we relax that assumption then multiple stable limit cycles are possible due to the periodicity of the interference field. The frequency of these oscillations is shown to depend sensitively on the laser power. Other complex motions exist for high laser power.

The analysis presented is applicable to any interferometrically driven MEMS device with a temperature dependent stiffness and static deflection, though clamped-clamped beams were chosen to analyze here due to their relatively simple structure. Physical

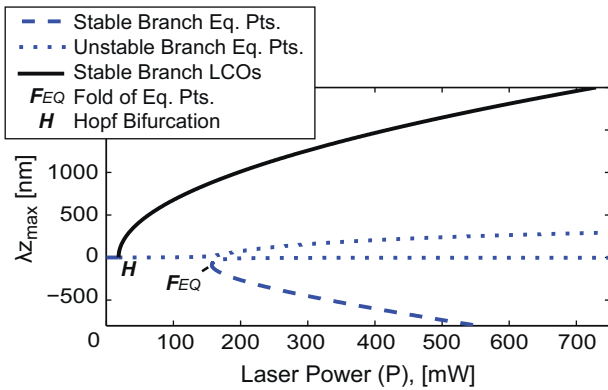


Fig. 11. Bifurcation diagram of the model equations assuming small displacement, where Eq. (3) has been expanded in a first-order Taylor series. Buckling has not been suppressed, but secondary Hopf bifurcations and folds of limit cycles have been lost. The approximate equations give a similar value for P_{Hopf} but not of the limit cycle amplitude or equilibrium solution.

devices exhibiting multiple stable limit cycles due to the phenomenon presented are expected to share some common characteristics:

- The need for a temperature dependent stiffness and deflection suggests the use of devices that can generate tension across the device, i.e. clamped–clamped beams or domes rather than cantilevers or disks.
- Damping has been shown to decrease the number of stable limit cycles accessible at a given power, thus devices would need to be high- Q .
- Stable limit cycles are seen to be separated in amplitude by $\Delta x \approx \lambda/2$. To permit n -stable limit cycles, devices must have an initial gap-to-substrate of greater than $n\lambda/2$ in order to prevent contact with the substrate. Excitation with a HeNe laser would require a gap of $\gtrsim 1 \mu\text{m}$ in order to see three limit cycles.

Although rigorously derived and analyzed, the results are expected only to present a qualitative picture of the dynamics of interferometrically driven MEMS devices, i.e. that multiple stable periodic motions are to be expected in large clamped–clamped beams and domes in low damping environments. Note that these motions are seen for low laser powers (below the buckling temperature). Above the buckling temperature, the frequency–compression relationship changes and the model may lose validity. A description of the bifurcation structure in this region of high laser power ($P > 168 \text{ mW}$ for the parameters used here) is presented and represents simply an analysis of the model, which suggests the possibility of period doubling, chaos and secondary Hopf bifurcations in the physical system.

Acknowledgments

This work is supported under NSF grant 0600174 and was performed in part at the Cornell NanoScale Facility, a member of the National Nanotechnology Infrastructure Network, which is supported by the National Science Foundation (Grant ECS-0335765). This work made use of the Integrated Advanced Microscopy and Materials facilities of the Cornell Center for Materials Research (CCMR) with support from the National Science Foundation Materials Research Science and Engineering Centers (MRSEC) program (DMR 1120296).

References

- Lin, R.T., Howe, A.P., Pisano, Microelectromechanical filters for signal processing, *Journal of Microelectromechanical Systems* 7 (3) (1998) 286–294, <http://dx.doi.org/10.1109/84.709645>.
- B.R. Ilic, D.A. Czaplowski, H.G. Craighead, P. Neuzil, C. Campagnolo, C.A. Batt, Mechanical resonant immunospecific biological detector, *Applied Physics Letters* 77 (2000) 450–452, <http://dx.doi.org/10.1063/1.127006>.
- A.M. Shkel, Type I and type II micromachined vibratory gyroscopes, in: *Proceedings of the IEEE/ION Plans*, 2006, pp. 586–593.
- N. Yazdi, F. Ayazi, K. Najafi, Micromachined inertial sensors, in: *Proceedings of the IEEE*, 1998, pp. 1640–1659.
- S. Lee, M.U. Demirci, C.T.-C. Nguyen, A 10-MHz micromechanical resonator pierce reference oscillator for communications, in: *Digest of Technical Papers, the 11th International Conference on Solid-State Sensors and Actuators (Transducers'01)*, 2001, pp. 10–14. <http://dx.doi.org/10.11152.6361>.
- X. Feng, C. White, A. Hajimiri, M. Roukes, A self-sustaining ultrahigh-frequency nanoelectromechanical oscillator, *Nature Nanotechnology* 3 (2008) 342–346, <http://dx.doi.org/10.1038/nnano.2008.125>.
- R. Langdon, D. Dowe, Photoacoustic oscillator sensors, in: *SPIE Conference on Fiber Optic Sensors*, 1987, pp. 86–93.
- O. Arcizet, P. Cohadon, T. Briant, M. Pinar, A. Heidmann, Radiation pressure cooling and optomechanical instability of a micromirror, *Nature* 444 (2006) 71–74, <http://dx.doi.org/10.1038/nature05244>.
- S. Gigan, H. Böhm, M. Paternostro, F. Blaser, G. Langer, J. Hertzberg, K. Schwab, D. Bäuerle, M. Aspelmeyer, A. Zeilinger, Self-cooling of a micromirror by radiation pressure, *Nature* 444 (2006) 67–70, <http://dx.doi.org/10.1038/nature05273>.
- M.W. Pruessner, T.H. Stievater, J.B. Khurgin, W.S. Rabinovich, An integrated waveguide-DBR microcavity opto-mechanical system, *Optics Express* 19 (22) (2011) 21904–21918, <http://dx.doi.org/10.1364/OE.19.021904>.
- T. Kippenberg, H. Rokhsari, T. Carmon, A. Scherer, K. Vahala, Analysis of radiation-pressure induced mechanical oscillation of an optical microcavity, *Physical Review Letters* 95 (2005) 033901, <http://dx.doi.org/10.1103/PhysRevLett.95.033901>.
- H. Rokhsari, T. Kippenberg, T. Carmon, K.J. Vahala, Radiation-pressure-driven micro-mechanical oscillator, *Optics Express* 13 (14) (2005) 5293–5301, <http://dx.doi.org/10.1364/OPEX.13.005293>.
- Q. Lin, J. Rosenberg, X. Jiang, K.J. Vahala, O. Painter, Mechanical oscillation and cooling actuated by the optical gradient force, *Physical Review Letters* 103 (2009) 103601, <http://dx.doi.org/10.1103/PhysRevLett.103.103601>.
- N. Stokes, R.M. Fatah, S. Venkatesh, Self-excitation in fiber-optic microresonator sensors, *Sensors and Actuators A* 21 (1990) 369–372, [http://dx.doi.org/10.1016/0924-4247\(90\)85073-D](http://dx.doi.org/10.1016/0924-4247(90)85073-D).
- A. Churenkov, Photothermal excitation and self-excitation of silicon microresonators, *Sensors and Actuators A* 39 (1993) 141–148, [http://dx.doi.org/10.1016/0924-4247\(93\)80211-X](http://dx.doi.org/10.1016/0924-4247(93)80211-X).
- K. Hane, K. Suzuki, Self-excited vibration of a self-supporting thin film caused by laser irradiation, *Sensors and Actuators A* 51 (1996) 179–182, [http://dx.doi.org/10.1016/0924-4247\(95\)01218-4](http://dx.doi.org/10.1016/0924-4247(95)01218-4).
- K.L. Aubin, M.K. Zalalutdinov, T. Alan, R.B. Reichenbach, R.H. Rand, A.T. Zehnder, J.M. Parpia, H.G. Craighead, Limit cycle oscillations in CW laser-driven NEMS, *Journal of Microelectromechanical Systems* 13 (6) (2004) 1018–1026, <http://dx.doi.org/10.1115.1.151.6977>.
- N. Stokes, R. Fatah, S. Venkatesh, Self-excited vibrations of optical microresonators, *Electronic Letters* 24 (13) (1988) 777–778.
- S. Kozel, V. Listvin, A. Churenkov, Photothermal self-excitation of mechanical microresonators, *Optics and Spectroscopy* 69 (3) (1991) 675–677.
- M.K. Zalalutdinov, A.T. Zehnder, A. Olkhovets, S.W. Turner, L. Sekaric, B.R. Ilic, D.A. Czaplowski, J.M. Parpia, H.G. Craighead, Autoparametric optical drive for micromechanical oscillators, *Applied Physics Letters* 79 (5) (2001) 695–697, <http://dx.doi.org/10.1063/1.1388869>.
- L. Sekaric, M.K. Zalalutdinov, R.B. Bhiladvala, A.T. Zehnder, J.M. Parpia, H.G. Craighead, Operation of nanomechanical resonant structures in air, *Applied Physics Letters* 81 (14) (2002) 2641–2643, <http://dx.doi.org/10.1063/1.1511287>.
- C.H. Metzger, K. Karrai, Cavity cooling of a microlever, *Nature* 432 (2004) 1002–1005, <http://dx.doi.org/10.1038/nature03118>.
- C.H. Metzger, M. Ludwig, C. Neuenhahn, A. Ortlieb, I. Favero, K. Karrai, F. Marquardt, Self-induced oscillations in an optomechanical system driven by bolometric backaction, *Physical Review Letters* 101 (2008) 133903, <http://dx.doi.org/10.1103/PhysRevLett.101.133903>.
- T. Sahai, R.B. Bhiladvala, A.T. Zehnder, Thermomechanical transitions in doubly-clamped micro-oscillators, *International Journal of Non-Linear Mechanics* 42 (4) (2007) 596–607, <http://dx.doi.org/10.1016/j.ijnonlinmec.2006.12.009>.
- D.W. Carr, L. Sekaric, H.G. Craighead, Measurement of nanomechanical resonant structures in single crystal silicon, *Journal of Vacuum Science and Technology B* 16 (6) (1998) 3821–3824, <http://dx.doi.org/10.1116/1.590416>.
- M.K. Zalalutdinov, J.M. Parpia, K.L. Aubin, H.G. Craighead, T. Alan, A.T. Zehnder, R.H. Rand, Hopf bifurcation in a disk-shaped NEMS, in: *Proceedings of the 2003 ASME Design Engineering Technical Conferences, 19th Biennial Conference on Mechanical Vibrations and Noise*, Chicago, IL, 2003, pp. 1759–1769.

- [27] M. Pandey, R.H. Rand, A.T. Zehnder, Perturbation analysis of entrainment in a micromechanical limit cycle oscillator, *Communications in Nonlinear Science and Numerical Simulation* 12 (2007) 1291–1301, <http://dx.doi.org/10.1016/j.cnsns.2006.01.017>.
- [28] M. Pandey, K.L. Aubin, M.K. Zalalutdinov, R.B. Reichenbach, A.T. Zehnder, R.H. Rand, H.G. Craighead, Analysis of frequency locking in optically driven MEMS resonators, *Journal of Microelectromechanical System* 15 (6) (2006) 1546–1554, <http://dx.doi.org/10.1109/JMEMS.2006.879693>.
- [29] D.B. Blocher, Optically driven limit cycle oscillations in MEMS, Ph.D. Thesis, Cornell University, Ithaca, 2012.
- [30] J.G. Easley, Nonlinear vibration of beams and rectangular plates, *Journal of Applied Mathematics and Physics* 15 (1964) 167–175, <http://dx.doi.org/10.1007/BF01602658>.
- [31] J.G. Easley, Large amplitude vibration of buckled beams and rectangular plates, *AIAA Journal* 2 (12) (1964) 2207–2209, <http://dx.doi.org/10.2514/3.2767>.
- [32] S.P. Timoshenko, *Vibration Problems in Engineering*, 3rd edition, D. Van Nostrand Company, Inc., 1955.
- [33] S. Bouwstra, B. Geijselaers, On the resonance frequency of microbridges, in: *Digest of Technical Papers, Solid-State Sensors and Actuators (Transducers'91)*, 1991, pp. 538–542, <http://dx.doi.org/10.1109/SENSOR.1991.148932>.
- [34] B.R. Ilic, S. Krylov, H.G. Craighead, Theoretical and experimental investigation of optically driven nanoelectromechanical oscillators, *Journal of Applied Physics* 107 (2010) 034311, [10.1063/1.3305464](https://doi.org/10.1063/1.3305464).
- [35] D.B. Blocher, A.T. Zehnder, R.H. Rand, S. Mukerji, Anchor deformations drive limit cycle oscillations in interferometrically transduced MEMS beams, *Finite Elements in Analysis and Design* 49 (1) (2012) 52–57, <http://dx.doi.org/10.1016/j.finel.2011.08.020>.
- [36] L. Sekaric, *Studies in NEMS: Nanoscale Dynamics, Energy Dissipation, and Structural Materials*, Ph.D. Thesis, Cornell University, 2003.
- [37] E.J. Doedel, R.C. Paffenroth, A.R. Champneys, T.F. Fairgrieve, Y.A. Kuznetsov, B.E. Oldeman, B. Sandstede, X. Wang, *AUTO 2000: Continuation and Bifurcation Software for Ordinary Differential Equations (with HomCont)*, 2002.
- [38] E.J. Doedel, Lecture notes on numerical analysis of nonlinear equations, in: B. Krauskopf, H.M. Osinga, J. Gálan-Vioque (Eds.), *Numerical Continuation Methods for Dynamical Systems*, Springer, 2007, pp. 1–49.
- [40] F.C. Moon, Experiments on chaotic motions of a forced nonlinear oscillator: strange attractors, *Journal of Applied Mechanics* 47 (3) (1980) 638–640, <http://dx.doi.org/10.1115/1.3153746>.
- [41] M. Pandey, R.H. Rand, A.T. Zehnder, Frequency locking in a forced Mathieu-vander Pol-Duffing system, *Nonlinear Dynamics* 54 (2008) 3–12, <http://dx.doi.org/10.1007/s11071-007-9238-x>.